SUPPLEMENTARY MATERIALS: MULTISCALE MODELS OF METALLIC PARTICLES IN NEMATIC LIQUID CRYSTALS*

THOMAS P. BENNETT†, GIAMPAOLO D'ALESSANDRO†, AND KEITH R. DALY‡

SM1. Transport theorems. The two versions of the transport theorem that we need are [SM1]

$$\frac{d}{dt}\int_\Omega F\,dS = \int_\Omega \frac{\partial F}{\partial t}\,dS + \int_{\partial\Omega} F(\boldsymbol{v}_b\cdot\hat{\boldsymbol{n}})\,dl, \tag{SM1.1}$$

and

$$\frac{d}{dt}\int_{\partial\Omega} F\,dl = \int_{\partial\Omega}\left[\frac{\partial F}{\partial t} + (\boldsymbol{v}_b\cdot\hat{\boldsymbol{n}})\hat{\boldsymbol{n}}\cdot\boldsymbol{\nabla}F - \boldsymbol{v}_b\cdot\hat{\boldsymbol{n}}\kappa F\right]dl, \tag{SM1.2}$$

where $\boldsymbol{v}_b$ is the velocity of the boundary and κ is the principal curvature of the boundary. From these equations we see that only the normal component of the boundary velocity contributes to the derivatives.

SM2. Electric field terms in the macroscopic alignment equation. In this appendix we give a detailed derivation of the expression (3.43) and (3.44) for the electric field terms in the macroscopic alignment equation (3.40). The starting point is the electrostatic term in equation (3.34), namely

$$\frac{\chi_a}{|\Omega|}\int_\Omega \boldsymbol{e}_0\,dS. \tag{SM2.1}$$

From equation (3.13h), following similar steps that lead to equation (3.15), we have that

$$e_k^{(0)} = \sqrt{2}\mathrm{Tr}\left[(\boldsymbol{\nabla}_{\boldsymbol{x}}\phi_0 + \boldsymbol{\nabla}_{\boldsymbol{y}}\phi_1)\otimes(\boldsymbol{\nabla}_{\boldsymbol{x}}\phi_0 + \boldsymbol{\nabla}_{\boldsymbol{y}}\phi_1)\,\mathcal{T}^{(k)}\right], \tag{SM2.2}$$

where we have used the result that ϕ_0 is independent of $\boldsymbol{y}$ to eliminate some of terms of the expansion. Substitution of this expression in equation (SM2.1) requires us to calculate three types of integrals. We consider these in turns.
The first integral is

$$\int_\Omega \boldsymbol{\nabla}_{\boldsymbol{x}}\phi_0\otimes\boldsymbol{\nabla}_{\boldsymbol{x}}\phi_0\,dS = |\Omega|\left(\boldsymbol{\nabla}_{\boldsymbol{x}}\phi_0\otimes\boldsymbol{\nabla}_{\boldsymbol{x}}\phi_0\right), \tag{SM2.3}$$

as $\phi(\boldsymbol{x})$ does not depend on the $\boldsymbol{y}$ coordinate.
The second integral is

$$\begin{aligned}\int_\Omega \boldsymbol{\nabla}_{\boldsymbol{x}}\phi_0\otimes\boldsymbol{\nabla}_{\boldsymbol{y}}\phi_1\,dS &= -\int_\Gamma \boldsymbol{\nabla}_{\boldsymbol{x}}\phi_0\otimes\boldsymbol{n}_0\phi_1\,dl\\ &= -\int_{\Omega_{\mathrm{np}}} \boldsymbol{\nabla}_{\boldsymbol{x}}\phi_0\otimes\boldsymbol{\nabla}_{\boldsymbol{y}}\phi_1\,dS,\end{aligned} \tag{SM2.4}$$

*KRD was funded by BB/J000868/1 and by ERC consolidation grant 646809 during the completion of this work.

†Mathematical Sciences, University of Southampton, Southampton, England, UK
‡Engineering Sciences, University of Southampton, Southampton, England, UK

where we have used the divergence theorem twice and Ω_{np} is the domain of the nanoparticle. The trick to simplify this equation is that the electrostatic field in a metallic particle is zero, i.e. $\boldsymbol{\nabla}\phi = 0$ inside any particle. The order η^0 terms of the expansion of this result is

$$\boldsymbol{\nabla}_{\boldsymbol{x}}\phi_0 + \boldsymbol{\nabla}_{\boldsymbol{y}}\phi_1 = 0. \tag{SM2.5}$$

Substituting equation (SM2.5) into (SM2.4) we obtain that

$$\int_\Omega \boldsymbol{\nabla}_{\boldsymbol{x}}\phi_0 \otimes \boldsymbol{\nabla}_{\boldsymbol{y}}\phi_1 \, dS = |\Omega_{\text{np}}| \left(\boldsymbol{\nabla}_{\boldsymbol{x}}\phi_0 \otimes \boldsymbol{\nabla}_{\boldsymbol{x}}\phi_0\right). \tag{SM2.6}$$

The integral of $\boldsymbol{\nabla}_{\boldsymbol{y}}\phi_1 \otimes \boldsymbol{\nabla}_{\boldsymbol{x}}\phi_0$ is treated exactly in the same way.
The third and last integral is

$$\int_\Omega \boldsymbol{\nabla}_{\boldsymbol{y}}\phi_1 \otimes \boldsymbol{\nabla}_{\boldsymbol{y}}\phi_1 \, dS = \int_\Omega \boldsymbol{\nabla}_{\boldsymbol{y}} R_k \otimes \boldsymbol{\nabla}_{\boldsymbol{y}} R_l \phi_{0,k} \phi_{0,l} \, dS, \tag{SM2.7}$$

where we have used equation (3.31) and indicate with $\phi_{0,k}$ the derivative of ϕ_0 with respect to x_k.

Substituting equations (SM2.3) and (SM2.6) into equation (SM2.1) gives equation (3.43) for the macroscopic electric field $\boldsymbol{e}_M$. The polarization term equation (3.44) is, instead, obtained by substituting equation (SM2.7).

SM3. Numerical simulation of the cell problems. Figure SM1 shows the solution of the cell problems for χ_k (3.28) and R_k (3.32) for an asymmetric particle both implemented using the general form PDEs package. The solutions have the form of horizontal and vertically oriented dipole potentials which are distorted by the particle shape, and, in the case of R_k, also by the alignment of the nematic. We solve cell problems (3.28) and (3.32) for a range of particle orientations parameterized by

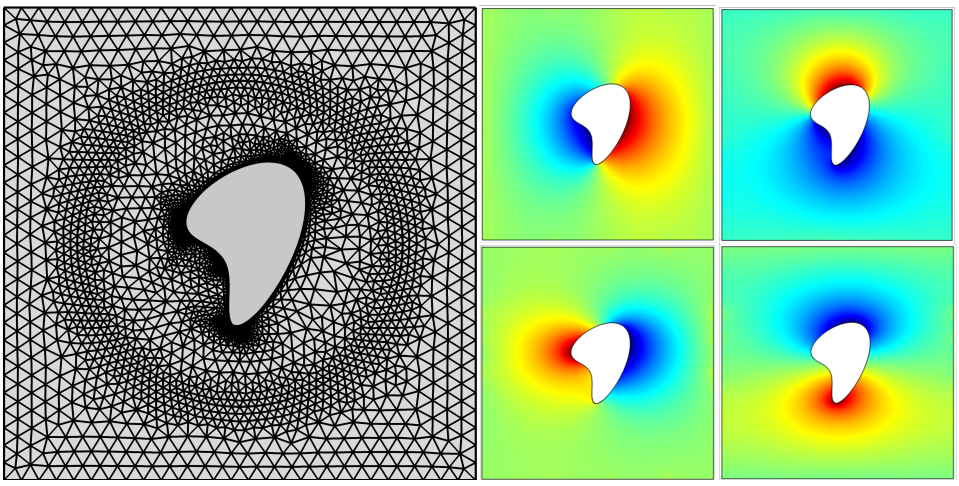

FIG. SM1. *(Left) Example of the meshing scheme used when solving* (2.25), (2.31), (2.29) *and*(2.32). *The particle motion is achieved by the entire circular region rotating as a solid body motion. This removes the need to re-mesh while solving. (right)Solution of the cell problems* (3.28) *and* (3.32) *for asymmetric particles. Plots show from top right proceeding clockwise:* χ_1, χ_2, R_2 *and* R_1. *The solution to these problems is used to compute the material parameters needed to solve the homogenized equations.*

the angle ψ, that measures the rotation with respect to the center of the cell. In the case of the cell problem (3.32) we also have to solve for a range of director orientations that we parameterize by an angle $\theta \in [0, \pi]$ that the director forms with the x_1 axis. Using the basis (2.3) and the definition (2.2) of the $\mathcal{Q}$-tensor the relation between θ and the director components $\boldsymbol{a}$ is $\boldsymbol{a} = S[-\cos(2\theta), \sin(2\theta)]$. Cubic spline interpolation is used to compute the effective material parameters and torques for generic $\psi \in [0, 2\pi]$ and $\theta \in [0, \pi]$.

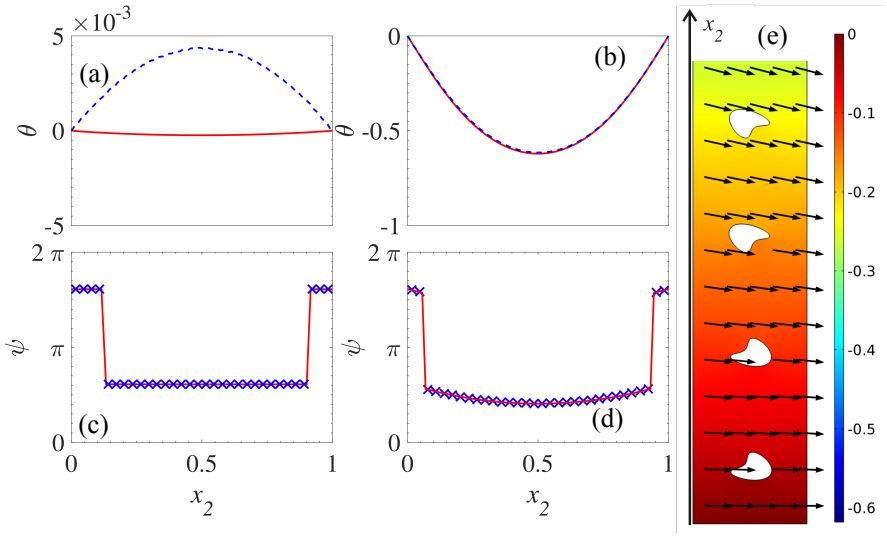

FIG. SM2. *Director (a,b) and particle (c,d) angle as a function of distance into the cell at $V = 0$ (a,c) and $V = 3$ (b,d) for $\tilde{\mu} = 10^{-6}$ Jm^{-2}. In all plots the red solid lines are the result of the homogenized/macroscopic equations, while the blue dashed lines and crosses are the solutions of the microscopic equations for $N = 32$ asymmetric particles of the same shape as in figure SM1. Panel (e) shows the particle orientation, director (arrows) and tilt angle (color) in the region close to $x_2 = 0$ at $V = 3$. The uniform director state at $V = 0$ (a) is only slightly disturbed by the presence of the particles (note that the vertical scale is 10^{-3}). At both voltage values the particle orientation flips by π as we move from away from the cell boundary (c,d).*

SM4. Numerical simulations of asymmetric particles. To further probe the validity of the theory we computed the alignment of $N = 32$ asymmetric particles, identical to those shown in figure SM1. The results for two different applied voltages, $V = \{0, 3\}$, are shown in figure SM2 for $\tilde{\mu} = 10^{-6}$ Jm^{-2}, which correspond to the stronger anchoring case illustrated in the left panel of figure 4.2. Once gain the agreement between macroscopic (red lines) and microscopic (blue dashed lines or crosses) models is excellent: the macroscopic model even manages to capture the jump discontinuity of the particle orientation as we move away from the boundary (panels (c) and (d) of figure SM2). To illustrate more clearly the change of alignment of the particles, panel (e) of figure SM2 plots the four particles closest to $x_2 = 0$ together with the director orientation.

There are a few items of note in this system that are not present in the case of symmetric particles. The first is that the microscopic model predicts that at $V = 0$ the director alignment is not uniformly flat, but has a very small deviation from $\theta = 0$ (panel (a) of figure SM2). This behavior is not captured by the macroscopic model. It is anticipated that the deviations are due to the incompatible symmetry between the particles and the nematic, and, the postulate that $\tilde{\mu}$ scales linearly with η. At

higher voltages (panel (b)) the agreement between the two models is excellent and the two curves are not distinguishable at the resolution of the plot. The second item to note is the jump discontinuity: this is not present for symmetric particles (for which ψ and $\psi + \pi$ are the same state) and if the number of particles is too small (it is not present for $N = 16$ particles). Finally, both the macroscopic and the microscopic system exhibit multi-stability: the first stationary state found depends on the initial conditions and the total number of particles.

REFERENCES

[SM1] S. Paolucci, *Continuum Mechanics and Thermodynamics of Matter*, Cambridge University Press, 2016.